Common Envelope Evolution on a Moving Mesh

Logan J. Prust[1]
[1]*Student (Department of Physics, University of Wisconsin-Milwaukee)*
Milwaukee, WI, USA

Abstract

The common envelope phase in binary star systems is simulated using the 3-D moving-mesh hydrodynamic code MANGA. Improvements to MANGA to improve accuracy and computation time are discussed. Two open questions in the physics of common envelope evolution are investigated. The effects of tidal forces present before the onset of a common envelope phase are explored by comparing simulations in which the giant star is initialized with varying degrees of rotation. The role of hydrogen recombination energy is investigated by using two different equations of state, only one of which includes the effects of recombination. Rotation is shown to increase the final binary separation, while recombination energy decreases the separation. Future improvements to MANGA to capture additional physics present in common envelopes are discussed.

1. Introduction

Common envelope evolution (CEE) is a phase during the life of a binary star system in which a giant star shares its gaseous envelope with a smaller companion object: a small star or a stellar remnant (for a review see Ivanova et al. 2013). The transfer of orbital energy and angular momentum from the giant's core and companion to the gas drives partial or complete ejection of the envelope from the system. This, in turn, causes the separation between the core and companion to decrease. This process is important for the formation of X-ray binaries, double white dwarfs, and double neutron stars, and may also be responsible for the merging black hole systems observed by Advanced LIGO (Ivanova et al. 2013). Despite its importance, CEE is not well understood, and this is due in part to the number of different physics that must be included as well as the range of time-scales involved. Furthermore, there is uncertainty as to whether the contributions from recombination and radiation energy should be included. Because of these challenges, our current

[1] The author is supported supported by the NASA Astrophysical Theory Program (ATP) through NASA grant NNH17ZDA001N-ATP. We use the Extreme Science and Engineering Discovery Environment (XSEDE), which is supported by National Science Foundation (NSF) grant No. ACI-1053575. We acknowledge the Texas Advanced Computing Center (TACC) at The University of Texas at Austin for providing HPC resources that have contributed to the research results reported within this paper (URL: http://www.tacc.utexas.edu). Computational resources supporting this work were also provided by the NASA High-End Computing (HEC) Program through the NASA Advanced Supercomputing (NAS) Division at the Ames Research Center. This material is based upon work supported by NASA under Award No. RFP19 7.0 issued through the Wisconsin Space Grant Consortium and the National Space Grant College and Fellowship Program. Any opinions, findings and conclusions or recommendations expressed in this material are those of the authors and do not necessarily reflect the views of the National Aeronautics and Space Administration. We thank Philip Chang for useful and detailed discussions.

understanding of CEE is limited at best. An important parameter here is the ejection efficiency: the fraction of the mass of the envelope that is ejected during the common envelope phase.

Generally, it is treated as a free parameter that one can vary to produce the desired results based on population synthesis modeling, a highly undesirable state of affairs.

In the presence of the different physics and time-scales, astronomers have mainly employed conserved quantities – energy and angular momentum – to roughly model CEE. These are known as the energy formalism (Webbink 1984) and the angular momentum (or γ) formalism (Nelemans et al. 2000). Because of the uncertainties in theoretical modeling of CEE, we bring numerical tools to bear. To perform 3-D simulations of CEE, two main approaches are used. The first is smooth particle hydrodynamics (SPH), where fluid quantities are determined from a finite sampling of nearby particles. SPH is computationally inexpensive and obeys conservation laws well, but the smoothing means that it has difficulty in handling discontinuities (i.e. shock waves). The other approach is Eulerian grid-based solvers, which are superior at capturing shocks but suffer from grid effects and violation of conservation laws (Springel 2010).

The defining numerical studies are those carried out by Passy et al. (2012), Ricker & Taam (2012) and Nandez et al. (2015). These simulations generally find a wide variation in efficiencies from about 5 to 100 per cent. Nandez et al. (2015) use a SPH code, Passy et al. (2012) use both a SPH and an Eulerian code and Ricker & Taam (2012) use an adaptive mesh refinement Eulerian code.

In recent years, a hybrid of these methods has been developed in an attempt to capture the best characteristics of both. This is the arbitrary Lagrangian-Eulerian (ALE) scheme, and software that use ALE schemes are known as moving mesh codes. In an ALE scheme, the mesh moves along with the fluid, combining the superior shock-capturing of grid-based solvers with the conservation properties of SPH. Springel (2010) described one such scheme that has proven successful, which is implemented in the code AREPO. The scheme constructs an unstructured mesh from an arbitrary distribution of points using a Voronoi tessellation. This guarantees that the mesh will be well defined, unique and continuously deformable; thus, finite volume methods can be applied in a manner similar to that of an Eulerian code. In addition, the lack of Galilean invariance in Eulerian codes is rectified if the mesh cells move along with the local flow. It has also been argued that ALE schemes are superior at capturing boundary layer instabilities such as Kelvin-Helmholtz instabilities (Springel 2010), though Lecoanet et al. (2016) cautioned that numerical noise can masquerade as solutions of such instabilities. Although AREPO was originally developed with cosmological simulations in mind, it has also been used in a number of problems including stellar mergers (Zhu et al. 2015) and common envelope evolution (Ohlmann et al. 2016). A moving-mesh hydrodynamic solver has also been developed for the N-body simulation code ChaNGa (Charm N-body GrAvity solver) (Jetley et al. 2008, 2010; Menon et al. 2015). This moving-mesh solver is known as MANGA, which is is described in detail by Chang et al. (2017). ChaNGa uses the

superior Charm++ framework for parallel computation rather than a custom MPI interface, allowing it to scale to up to 500,000 cores (Menon et al. 2015). MANGA has been validated on several test problems, including the Sod shock tube, Sedov-Taylor blast wave, Gresho-Chan vortex, and Evrard collapse. It was also successfully applied to hydrostatic stars and stellar mergers (Chang et al. 2017). In Prust & Chang (2019, hereinafter PC19), we incorporated individual timesteps into MANGA and showed that this results in a speedup of a factor of 4 to 5 for a CEE simulation.

One of the key advantages of MANGA over similar codes is its ability to seamlessly switch between various numerical schemes and equations of state (EOS), which makes it easy to compare physical models (Chang et al. 2017). An adiabatic EOS for the gas, $P \propto \rho^{\gamma}$ where γ is the adiabatic index, was originally implemented in MANGA. This simple EOS has been used in a number of simulations by previous groups (Ricker & Taam 2012; Ohlmann et al. 2016), which found an ejection efficiency of only 5% to 25%. This differs from the large implied values of ejection efficiency from observational studies, which suggests the existence of some additional energy not accounted for in the simulations. One candidate for this is the energy provided by hydrogen recombination in the outer envelope. More realistic EOSs can allow us to capture the additional effects of recombination. For instance, Nandez et al. (2015) found that including recombination energy leads to a complete ejection of the envelope. However, Nandez et al. (2015) also found an ejection efficiency of 50% without recombination energy, which is much higher than in previous studies. This makes it easier to eject the rest of the envelope with the inclusion of recombination energy. We suspect the reason for their high efficiency is the low resolution of their simulations and relatively primitive numerical schemes. To this end, we have also adapted the EOS implemented in the stellar evolution code MESA (Paxton et al. 2011, 2013, 2015, 2018, 2019) for use in MANGA, as described in PC19. The MESA EOS relies on several equations of state relevant over the different regimes of stellar structure and allows us to capture the effects of hydrogen recombination energy.

During the phase leading up to CEE, tidal forces from the companion on the envelope are expected to spin up the rotation of the envelope (Soker 1996) to a significant fraction of its breakup velocity. However, this rotation is not taken into account by most work on CEE. It is not clear to what degree the rotation has accelerated by the time the common envelope phase begins, but MacLeod et al. (2018) show that the giant nearly corotates with the binary orbit at the onset of CEE. We use the velocity profile of MacLeod et al. (2018) to set an initial condition on the corotation of the giant and treat this as a parameter to be tuned in our simulations.

We have organized this paper as follows. In section 2, we summarize the algorithm of MANGA and describe the initial conditions for our simulations. In section 3, we describe the results of our simulations of a 2 M red giant and a 1 Mcompanion. We discuss our results and future directions in section 4.

2. Methodology

2.1. Summary of the MANGA algorithm The ALE algorithm that is implemented in MANGA is briefly summarized as follows. We refer the reader to Chang et al. (2017) and PC19 for detailed discussions. MANGA solves the Euler equations, which written in conservative form are

$$\frac{\partial \rho}{\partial t} + \boldsymbol{\nabla} \cdot \rho \boldsymbol{v} = 0 \tag{1}$$

$$\frac{\partial \rho \boldsymbol{v}}{\partial t} + \boldsymbol{\nabla} \cdot \rho \boldsymbol{v}\boldsymbol{v} + \boldsymbol{\nabla} P = -\rho \boldsymbol{\nabla} \Phi \tag{2}$$

and

$$\frac{\partial \rho e}{\partial t} + \boldsymbol{\nabla} \cdot (\rho e + P)\, \boldsymbol{v} = -\rho \boldsymbol{v} \cdot \boldsymbol{\nabla} \Phi \tag{3}$$

where ρ is the density, v is the fluid velocity, Φ is the gravitational potential, $e = \epsilon + v^2/2$ is the specific energy, is the internal energy and $P(\rho, \epsilon)$ is the pressure. Eq. 1 to 3 can be written in a compact form by introducing a state vector $U = (\rho, \rho v, \rho e)$:

$$\frac{\partial U}{\partial t} + \nabla \cdot F = S, \tag{4}$$

where $F = (\rho v, \rho v v + P, (\rho e + P) v)$ is the flux function and $S = (0, -\rho \nabla \Phi, -\rho v \cdot \nabla \Phi)$ is the source function. To solve Eq. 4, we adopt the same finite volume strategy as Springel (2010). For each cell, the integral over the volume of the ith cell V_i defines the charge of the ith cell to be Z

$$\boldsymbol{U}_i = \int_{V_i} \boldsymbol{\mathcal{U}} dV = \boldsymbol{\mathcal{U}}_i V_i. \tag{5}$$

We then use Gauss' theorem to convert the volume integral over the divergence of the flux in Eq. 4 to a surface integral

$$\int_{\partial V_i} \boldsymbol{\nabla} \cdot \boldsymbol{\mathcal{F}} dV = \int_{\partial V_i} \boldsymbol{\mathcal{F}} \cdot \hat{\boldsymbol{n}} dA, \tag{6}$$

where ∂V_i is the boundary of the cell. We now take advantage of the fact that the volumes are Voronoi cells with a finite number of neighbours to define an integrated flux

$$\sum_{j \in \text{neighbors}} \boldsymbol{F}_{ij} A_{ij} = \int_{\partial V_i} \boldsymbol{\mathcal{F}} \cdot \hat{\boldsymbol{n}} dA, \tag{7}$$

where F_{ij} and A_{ij} are the average flux and area of the common face between cells i and j. The discrete time evolution of the charges in the system is given by

$$\boldsymbol{U}_i^{n+1} = \boldsymbol{U}_i^n + \Delta t \sum_j \hat{\boldsymbol{F}}_{ij} A_{ij} + \Delta t \boldsymbol{S}_i, \tag{8}$$

where $\hat{F}_{ij}$ is an estimate of the half time-step flux between the initial U^n_i and final states U^{n+1}_i and $S_i^{(n+1/2)} = \int_R i \, SdV$ is the time-averaged integrated source function.

We estimate the flux $\hat{F}_{ij}$ across each face as follows.

(i) Use the gradient estimates at the initial time-step to predict the half time-step cell-centered values.

(ii) Drift the cells a half time-step and rebuild the Voronoi tessellation at the half time-step.

(iii) Estimate the half time-step state vector (in the rest frame of the moving face) at the face center ($\tilde{r}_{ij}$) between the neighboring i and j cells by linear reconstruction.

(iv) Estimate the (half time-step) velocity $\tilde{w}_{ij}$ of the face, and boost the state vector from the "lab" frame (the rest frame of the simulation box) to the rest frame of the face to find the flux along the normal of the face. I.e., in the direction from i to j.

(v) Estimate the flux $\hat{F}_{ij}$ across the face using an HLLC or HLL (or HLLD for MHD, Chang, in preparation) approximate Riemann solver implemented following Toro (2009).

(vi) Boost the solved flux back into the "lab" frame.

We can then use the estimated fluxes to time-evolve the charges U_i following Eq. 8 using the full time-step δt and apply changes owing to the source terms.

2.2. Simulation setup We now outline the development of appropriate initial conditions for CEE simulations in MANGA. The reader is referred to PC19 for a detailed discussion. We first use MESA to evolve a 2 M star with metallicity $Z = 0.02$ from the pre-main sequence to the red giant phase. We stop when the star reaches 52 R with a helium core mass of 0.36 M. From the MESA output, we take the entropy and hydrogen fraction. For the core, we take the total mass at a density that is 50 times greater than the mean density of the red giant, giving a core mass $M_c = 0.379\ \mathrm{M}_\odot$. This corresponds to a core radius $R_c = 1.99\ \mathrm{R}_\odot$, which we use as the core gravitational softening length h. For all particles present regardless of type, MANGA uses spline softening to soften the gravitational forces within radius h of the particle. Because of the great difference in density between the helium core and the hydrogen envelope, we model the core as a dark matter particle with mass M_c and softening radius of R_c. We then take the entropy profile and construct a star of mass $M - M_c$, with an entropy profile which matches that of the original star and contains a dark matter particle core. This yields a radial profile of density, temperature and hydrogen fraction that can be mapped to a particle (mesh-generating point) profile.

We construct an appropriate particle mesh for the star from a pre-computed glass distribution of points embedded in a 3-D cube. We periodically replicate this glass distribution to produce sufficient numbers of particles. We assume that each particle is of equal volume and rescale them

to the appropriate mass based on the computed $M(r)$ from MESA. These particles are also endowed with the radially interpolated temperature and hydrogen fraction. The total number of particles representing the star is 3×10^5. Outside of the star, we include a low density atmosphere of 10^{-13} g cm^{-3} with temperature 10^5 K that extends out to the total box size of 3.5×10^{14} cm (^{5000} R$_\odot$), with periodic boundary conditions at its edges. The total number of particles in the simulation box is 8×10^5. To lower the computational cost, we use a mesh refinement algorithm to decrease the number of gas particles in the atmosphere far from the star. We define a scale factor $S(r) = (r/R_*)^n$ where R_* is the radius of the star, r is the spherical radius and n is an adjustable parameter which we have set to $n = 2/3$ in this case. Starting with the same uniform glass distribution as for the star, the linear spacing between particles is increased by S and their mass is increased by S^3, preserving the external density.

We represent the 1 M companion as a dark matter particle in an initially circular Keplerian orbit at the red giant radius^a = 52 R$_\odot$. Although this neglects the evolution of the binary prior to CEE, we compensate by altering the dynamics of the giant. We have implemented the corotation between the envelope rotation and orbital motion into our simulations following the scheme of MacLeod et al. (2018). Within the envelope, we assume rigid body rotation and initialize the velocity as

$$v\varphi = f\mathrm{cr}\Omega\mathrm{orb}R\mathrm{cyl}, \tag{9}$$

but give the atmosphere a velocity

$$v_\phi = \frac{f_{\rm cr}\Omega_{\rm orb}R_*^2\sin^2(\theta)}{R\mathrm{cyl}} \tag{10}$$

Here, $f_{\rm cr}$ is an adjustable parameter, φ is the azimuthal angle, θ is the polar angle, $\Omega_{\rm orb}$ is the orbital frequency of the red giant and companion, R_* is the radius of the giant and $R_{\rm cyl}$ is the cylindrical radius from the rotation axis of the giant. We note that Eq. 9 and 10 ensure that the velocity is continuous at the surface of the giant.

Here, we run two simulations investigating the effect of corotation on the parameters of the final binary system, both using the MESA EOS. We initialize the giant in two different states of corotation, 95 per cent corotation ($f_{cr} = 0.95$) and 0 per cent corotation ($f_{cr} = 0$). We note that the 95 per cent corotation case follows the simulations of Ohlmann et al. (2016) and Ricker & Taam (2012). The choice to set f_{cr} to less than unity is also motivated by MacLeod et al. (2018) who found that orbital angular momentum lost by the companion prior to the onset of a common envelope phase does not necessarily go into spinning up the envelope, leading to a desynchronization between the orbital frequencies of the companion and envelope. We also run two simulations the determine the effect of hydrogen recombination energy on CEE. This is accomplished by using two different equations of state: the adiabatic EOS and the MESA EOS. For the recombination study, both giants are initially non-rotating.

3. Results

3.1. Corotation We first discuss the simulations with varying degrees of corotation. Starting with the above initial conditions, we simulate the binary for 240 d and show several density

projections at t = 1, 10, 30, 75, 120 and 240 d for the simulation with 95 per cent corotation in Fig. 1. In both simulations, the companion experiences an initial plunge into the envelope of the giant that lasts about 15 days, throwing off a large tidal tail (Fig. 1 upper center) and greatly decreasing the separation between the companion and core. The companions then continue to spiral in as their orbital energy is transferred to the gas; the spiral shocks facilitating this transfer can be seen in the projections (Fig. 1 upper right). We see smaller tidal tails thrown off at t = 75 d (lower left) and t = 120 d (lower center), as well as several others. The simulation ends well before the outflow reaches the edge of the simulation box.

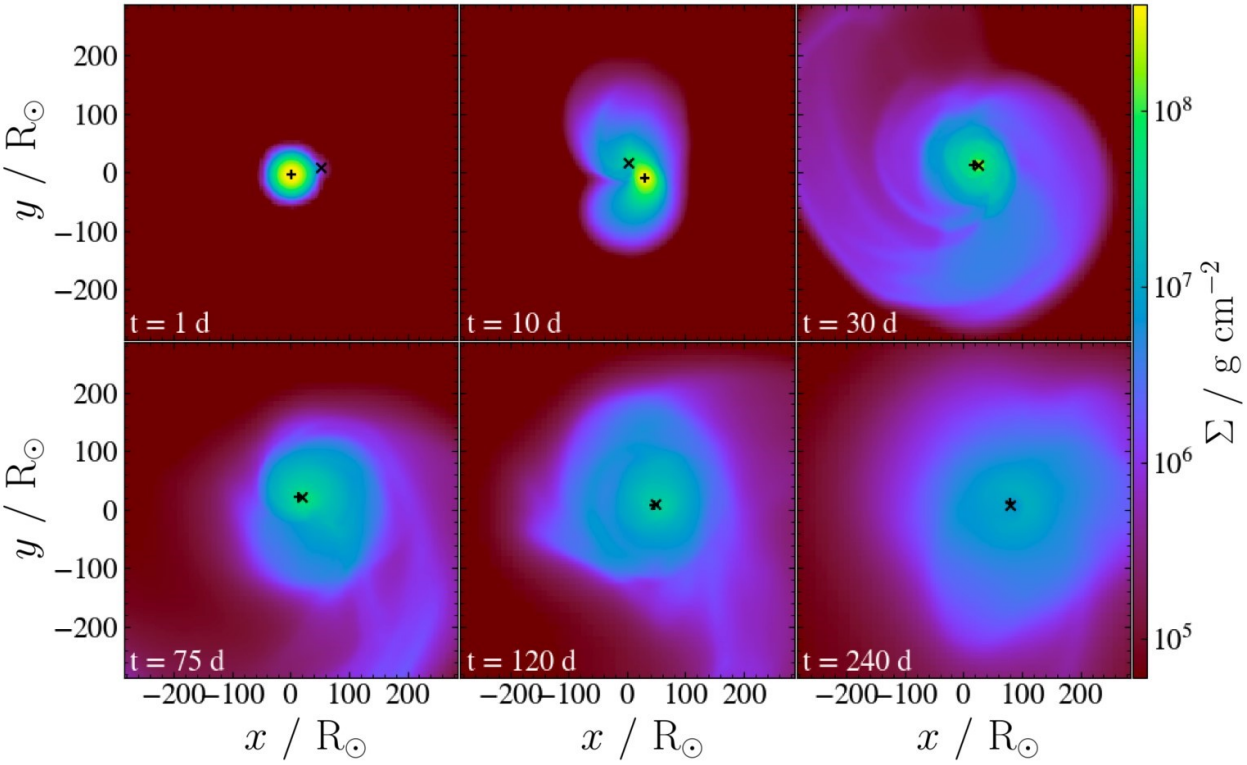

Figure 1: Density projections Σ with 95 per cent corotation. The + sign marks the red giant core and the × marks the companion.

The total energy of each gas particle is given by

$$E_{\mathrm{tot,i}} = m_i[\frac{1}{2}(\boldsymbol{v}_i - \boldsymbol{v}_{\mathrm{CM}})^2 + \phi_i + I_{e,i}] \tag{11}$$

(Nandez et al. 2015), where m_i, v_i, v_{CM}, φ_i and $I_{e,i}$ are the mass, velocity, center of mass velocity of the bound material, gravitational potential and specific internal energy of each particle. Gas particles with a negative total energy are bound to the binary, while those with a positive total energy are unbound. The kinetic energy is computed relative to the velocity of the center of mass (CM) of the *bound* matter; that is, the bound gas as well as both dark matter particles. However, because the total energy is needed in order to determine which gas particles are bound, we use an iterative scheme to find the velocity of the CM, described in PC19. With the total energies of all particles known, we can find the mass of the unbound gas $m_{\mathrm{g,u}}$ as a fraction of the total mass of the envelope m_{env},

$$f_{\rm unb} = \frac{m_{\rm g,u}}{m_{\rm env}}, \tag{12}$$

which we refer to as the ejection efficiency. This is shown in Fig. 2. Qualitatively, the simulations are very similar in this regard. They show a large ejection of gas during the initial plunge as well as during the ejection of additional tidal tails. We find that the system set into corotation consistently exhibits a higher ejection efficiency, likely owing to the inclusion of additional kinetic energy and angular momentum. Matter continues to be ejected up until the end of the simulation period, ending with an efficiency of 66 per cent with corotation and 63 per cent for no corotation.

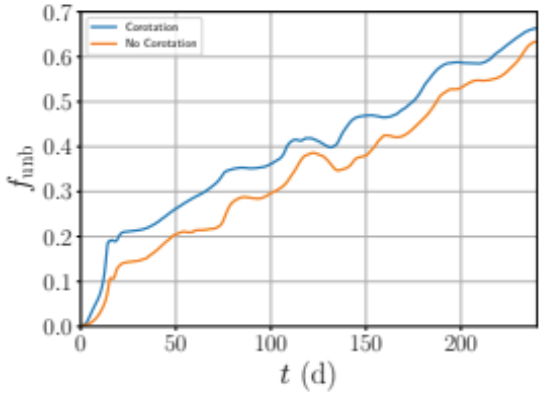

Figure 2: The fraction of mass of the envelope that has acquired enough energy to be unbound from the system in our corotation study. The large tidal tail thrown off in the initial plunge can be seen from 0 to 15 d, with several subsequent tails.

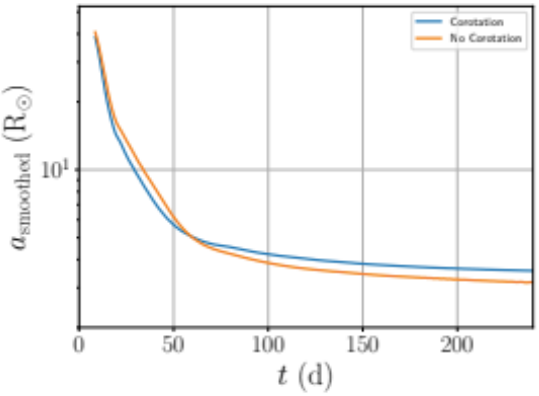

Figure 3: Separation a between the stellar core and companion in each case, smoothed over time and shown on a logarithmic scale for ease of reading. Here we can see that the simulation with no corotation results in a smaller separation by 0.4 $R_\odot$.

The separations between the stellar core and companion are shown in Fig. 3. For ease of reading, we show the separations on a logarithmic scale and smooth them over a period of 15 d. That is, each separation a_i is taken to be the average of all separations within an interval of 15 d centered on a_i. After one orbit, both binaries have reduced their orbital separation to less than half the initial separation, and they continue to spiral in at a slower rate. Although the simulation with corotation initially falls to a smaller separation, it is eventually surpassed by its counterpart. The final (smoothed) separations are 3.6 R with corotation and 3.2 R with no corotation.

3.2. Recombination energy We again simulate the binary for 240 d using the adiabatic EOS and the MESA EOS. The ejection efficiency, calculated using Eq. 11 and 12, is shown in Fig. 4 for both simulations. We see that the ejection efficiency is smoother for the adiabatic case, suggesting that the tidal tails are not as efficient at ejecting mass from the binary. We also find the surprising result that despite being similar at early times, the adiabatic simulation exhibits a much higher final ejection efficiency than the MESA version. The adiabatic and MESA simulations end with 92 per cent and 63 per cent of the envelope ejected, respectively. One would expect that the additional energy injected into the gas through recombination would help to eject gas from the system, but apparently there are other factors at play. One possible explanation is that the stellar structure differs significantly between the two equations of state. This change in structure could then alter the dynamics of the companion as it spirals in.

Fig. 5 shows the separations for the recombination energy study. Corresponding to the higher ejection efficiency, we see that the adiabatic simulation ends with a smaller final separation, meaning that more of the orbital energy has been transferred to the gas. Whereas the MESA simulation ends with a separation greater than 3 R, the adiabatic case continues to shrink its orbit to$\approx 2.5\ \mathrm{R}_\odot$.

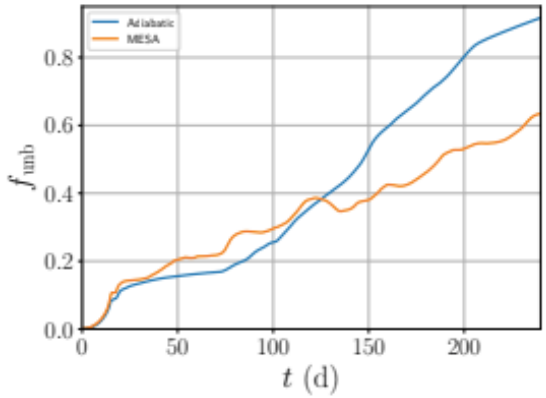

Figure 4: The fraction of mass of the envelope that has acquired enough energy to be unbound from the system in our recombination study. The adiabatic case unbinds more of its envelope than the MESA case after $t \approx 125$ d.

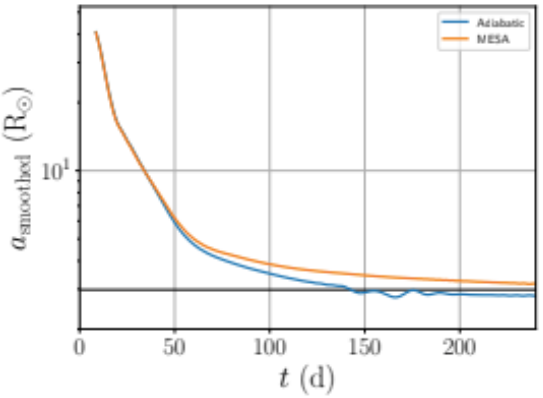

Figure 5: Smoothed separation a between the stellar core and companion in our recombination study. The black horizontal line lies at 3 $\mathrm{R}_\odot$, the sum of the initial gravitational softening lengths of the core and companion.

Because the separation in the adiabatic case is so small, we encountered issues with the gravitational softening lengths h. The softening lengths of the core and companion are and 1 R, respectively. Thus, if the separation is less than the combined softening length, violations of Newton's third law can occur. That is, the gravitational forces exerted on the dark matter particles by one another are not necessarily equal and opposite. To combat this, we have developed a method by which h can be changed mid-simulation. At $t = 100$ d, we change the softening length of the core to 1 R for the remainder of the simulation. This results in a change in the core-gas gravitational potential energy of 0.11 per cent. We do not believe that this change in h is responsible for the surprisingly large ejection efficiency because the change in energy associated with modifying h is very small. We also ran the simulation without modification of h and found similar behavior.

3.3. Agreement with observation Our results can be linked to observations using surveys of binaries containing low-mass white dwarfs. Gianninas et al. (2014) have found systems (such as J0755+4800, J1151+5858, and J1518+0658) with primary masses in the range of 0.18 to 0.41 $M_\odot$, consistent with the mass of our core, with companion masses $\geq 0.6\ M_\odot$ and separations of $\sim 3\ R_\odot$. These systems are consistent with our simulations, although the observed systems have ejected their envelopes. It is not clear from our simulations whether the envelopes will be completely ejected and how the orbital parameters would differ in that case.

4. Discussion

In this work, we investigate the physics of CEE using the moving-mesh code MANGA. We generate initial conditions for our simulations by using MESA to evolve a pre-main sequence star to the red giant phase before placing a companion on its surface in a circular orbit. We run simulations of a 2 M giant with a 1 M companion for 240 d.

Prior to the onset of CEE, the giant is expected to be spun up by tidal forces from the companion, and we study this by initializing the giant with rotation in our simulations. In two of our simulations, we take the rotation of the envelope to be either 95 or 0 per cent of the (initial) orbital frequency. After 240 d, we find that the orbital separation of the red giant core and the companion has been reduced to 3.6 R and 3.2 R, respectively. This is a reduction in the separation by a factor of 15. Most of the envelope is ejected (66 and 63 per cent, respectively), which is larger than many of the results of previous work. However, 3-D numerical computations of CEE have found a wide variance in the ejection efficiency of the envelope. Early work (for example, Livio & Soker 1988) found envelope ejection efficiencies from about 10 to 80 per cent. However, the resolutions of these early simulations were poor. More recent work (Passy et al. 2012; Ricker & Taam 2012; Nandez et al. 2015; Ohlmann et al. 2016) also find a large variance in the efficiencies (about 5 to 100 per cent). We find that the inclusion of corotation results in a larger final separation as well as a larger ejection efficiency. This is thought to be due to the inclusion of additional kinetic energy and angular momentum in the initial conditions. The differences in the final binary due to corotation are significant, particularly with regard to the separation. This suggests that corotation cannot be ignored and should be included in future simulations of CEE.

It has also been suggested that inclusion of recombination energy would result in more efficient expulsion of the envelope (see the review by Ivanova 2017). We note that this point is controversial, as Soker and collaborators have claimed that the energy from recombination is easily transported away either by radiation or convection (Sabach et al. 2017; Soker et al. 2018). However, Ivanova (2018) reached the opposite conclusion, that the fraction of recombination energy transported away from the regions in which recombination takes place is negligible. We include recombination energy in our simulations through the use of the MESA EOS and test it against the simpler adiabatic EOS. Nandez et al. (2015) found that between 50 and 100 per cent of the envelope mass is ejected in their simulations, depending on the inclusion of recombination energy. Although our ejection efficiencies are similarly high, we find the opposite result that the adiabatic EOS gives a larger efficiency and a correspondingly smaller separation. This unexpected result is likely due to the fact that changing the EOS not only changes the treatment of recombination, but also changes the structure of the star. This change in structure could then alter the dynamics of the companion as it spirals in. However, it is also possible that radiative cooling could be important in CEE, particularly with regard to the energy injected during recombination.

Radiation physics is currently being implemented into MANGA (Chang, Davis & Jiang, in preparation), and when this is complete we will incorporate it into our CEE simulations.

We note here that other processes may also aid the expulsion of the envelope. Much recent work have been focused on energy and momentum injection from jets produced by accretion onto the companion (for example, Lopez-C´ amara´ et al. 2018). In addition, the transition from laminar flow to accretion flows around the companion star can be complicated and also provide another mechanism by which orbital energy is dissipated (MacLeod et al. 2017). Much of the work have focused on Bondi-Littleton-Hoyle type accretion around a point mass. However, a typical accretor has a physical scale of a solar radius, which gives it a nontrivial cross section in a red giant envelope. Typically, we can show that a 1 R accretor encounters 10 to 50 per cent of the envelope in one orbit. This hydrodynamic interaction may play a significant role in the evolution of the common envelope and the binary orbit.

To date, all simulations of CEE – including those presented here – have assumed that the size of the companion object is negligibly small compared to the red giant envelope, and have modeled the companion as a point particle. This assumption is appropriate if the companion is a black hole or neutron star, but is not generally valid. The implementation of moving boundary conditions into MANGA (Prust, in preparation) will allow us to model the companion as a spherical boundary of arbitrary size. This will more accurately model the shock waves created by the motion of the companion through the envelope, and can also be used to implement a model for accretion onto the companion. Preliminary simulations of CEE using this methodology are encouraging, but have only been tested with low resolution at the time of writing. High-resolution simulations of CEE using the MESA EOS could shed light on the effects of companion size and inform future work. In particular, the drag force on the companion is expected to depend upon the size of the companion, and could alter the dynamics of the spiral-in phase (Chamandy et al. 2019).

Acknowledgments

We thank Philip Chang for useful and detailed discussions. We are supported by the NASA Astrophysical Theory Program (ATP) through NASA grant NNH17ZDA001N-ATP. We use the Extreme Science and Engineering Discovery Environment (XSEDE), which is supported by National Science Foundation (NSF) grant No. ACI-1053575. We acknowledge the Texas Advanced Computing Center (TACC) at The University of Texas at Austin for providing HPC resources that have contributed to the research results reported within this paper (URL: http://www.tacc.utexas.edu). We use the YT software platform for the analysis of the data and generation of plots in this work (Turk et al. 2011). Computational resources supporting this work were also provided by the NASA High-End Computing (HEC) Program through the NASA Advanced Supercomputing (NAS) Division at the Ames Research Center. This material is based upon work supported by NASA under Award No. RFP19 7.0 issued through the Wisconsin Space Grant Consortium and the National Space Grant College and Fellowship Program. Any opinions, findings and conclusions or recommendations expressed in this material are those of the authors and do not necessarily reflect the views of the National Aeronautics and Space Administration.

References

Chamandy, L; Blackman, EG; Frank, A; Carroll-Nellenback, J; Zou, Y; Tu, Y. “How Drag Force Evolves in Global Common Envelope Simulations,” *arXiv e-prints*, 2019, p. arXiv:1908.06195. https://ui.adsabs.harvard.edu/abs/2019arXiv190806195C

Chang, P; Wadsley, J; Quinn, T. “A Moving Mesh Hydrodynamics Solver for ChaNGa,” *accepted to MNRAS*, 2017

Gianninas, A; Dufour, P; Kilic, M; Brown, WR; Bergeron, P; Hermes, JJ. “Precise Atmospheric Parameters for the Shortest-period Binary White Dwarfs: Gravitational Waves, Metals, and Pulsations,” *ApJ*, v. 794, 2014, p. 35. https://ui.adsabs.harvard.edu/#abs/2014ApJ...794...35G

Ivanova, N. “Common envelope: progress and transients,” preprint (arXiv:1706.07580), 2017. http://adsabs.harvard.edu/abs/2017arXiv170607580I

—. “On the Use of Hydrogen Recombination Energy during Common Envelope Events,” *ApJ*, v. 858, 2018, p. L24. https://ui.adsabs.harvard.edu/abs/2018ApJ...858L..24I

Ivanova, N; Justham, S; Chen, X; De Marco, O; Fryer, CL; Gaburov, E; Ge, H; Glebbeek, E; Han, Z; Li, XD; Lu, G; Marsh, T; Podsiadlowski, P; Potter, A; Soker, N; Taam, R; Tauris, TM; van den Heuvel, EPJ; Webbink, RF. “Common envelope evolution: where we stand and how we can move forward,” *A&A Rev.*, v. 21, 2013, p. 59. http://ukads.nottingham.ac.uk/abs/2013A%26ARv..21...59I

Jetley, P; Gioachin, F; Mendes, C; Kale, LV; Quinn, TR. “”massively parallel cosmological simulations with changa”,” *Proceedings of IEEE International Parallel and Distributed Processing Symposium*, 2008

Jetley, P; Wesolowski, F; Gioachin, F; Kale, LV; Quinn, TR. “”scaling hierarchical n-body simulations on gpu clusters”,” *Proceedings of the 2010 ACM/IEEE International Conference for High Performance Computing*, 2010

Lecoanet, D; McCourt, M; Quataert, E; Burns, KJ; Vasil, GM; Oishi, JS; Brown, BP; Stone, JM; O’Leary, RM. “A validated non-linear Kelvin-Helmholtz benchmark for numerical hydrodynamics,” *MNRAS*, v. 455, 2016, p. 4274–4288. http://adsabs.harvard.edu/abs/2016MNRAS.455.4274L

Livio, M; Soker, N. “The common envelope phase in the evolution of binary stars,” *ApJ*, v. 329, 1988, p. 764–779. http://adsabs.harvard.edu/abs/1988ApJ...329..764L

Lopez-C´ amara,´ D; De Colle, F; Moreno Mendez,´ E. “Self-regulating jets during the Common Envelope phase,” preprint (arXiv:1806.11115), 2018, p. arXiv:1806.11115. https://ui.adsabs.harvard.edu/abs/2018arXiv180611115L

MacLeod, M; Antoni, A; Murguia-Berthier, A; Macias, P; Ramirez-Ruiz, E. “Common Envelope Wind Tunnel: Coefficients of Drag and Accretion in a Simplified Context for Studying Flows around Objects Embedded within Stellar Envelopes,” *ApJ*, v. 838, 2017, p. 56. https://ui.adsabs.harvard.edu/abs/2017ApJ...838...56M

MacLeod, M; Ostriker, EC; Stone, JM. “Runaway Coalescence at the Onset of Common Envelope Episodes,” *ApJ*, v. 863, 2018, p. 5. https://ui.adsabs.harvard.edu/#abs/2018ApJ...863....5M

Menon, H; Wesolowski, L; Zheng, G; Jetley, P; Kale, L; Quinn, T; Governato, F. “Adaptive techniques for clustered N-body cosmological simulations,” *Computational Astrophysics and Cosmology*, v. 2, 2015, p. 1. http://adsabs.harvard.edu/abs/2015ComAC...2....1M

Nandez, JLA; Ivanova, N; Lombardi, JC. “Recombination energy in double white dwarf formation,” *MNRAS*, v. 450, 2015, p. L39–L43. http://adsabs.harvard.edu/abs/2015MNRAS.450L..39N

Nelemans, G; Verbunt, F; Yungelson, LR; Portegies Zwart, SF. “Reconstructing the evolution of double helium white dwarfs: envelope loss without spiral-in,” *A&A*, v. 360, 2000, p. 1011–1018. http://adsabs.harvard.edu/abs/2000A%26A...360.1011N

Ohlmann, ST; Ropke, FK; Pakmor, R; Springel, V. “Hydrodynamic Moving-mesh Simulations of the Common Enve- ¨ lope Phase in Binary Stellar Systems,” *ApJ*, v. 816, 2016, p. L9. http://adsabs.harvard.edu/abs/2016ApJ...816L...9O

Passy, JC; De Marco, O; Fryer, CL; Herwig, F; Diehl, S; Oishi, JS; Mac Low, MM; Bryan, GL; Rockefeller, G. “Simulating the Common Envelope Phase of a Red Giant Using Smoothed-particle Hydrodynamics and Uniformgrid Codes,” *ApJ*, v. 744, 2012, p. 52. http://adsabs.harvard.edu/abs/2012ApJ...744...52P

Paxton, B; Bildsten, L; Dotter, A; Herwig, F; Lesaffre, P; Timmes, F. “Modules for Experiments in Stellar Astrophysics (MESA),” *ApJS*, v. 192, 2011, p. 3. http://adsabs.harvard.edu/abs/2011ApJS..192....3P

Paxton, B; Cantiello, M; Arras, P; Bildsten, L; Brown, EF; Dotter, A; Mankovich, C; Montgomery, MH; Stello, D; Timmes, FX; Townsend, R. “Modules for Experiments in Stellar Astrophysics (MESA): Planets, Oscillations, Rotation, and Massive Stars,” *ApJS*, v. 208, 2013, p. 4. http://adsabs.harvard.edu/abs/2013ApJS..208....4P

Paxton, B; Marchant, P; Schwab, J; Bauer, EB; Bildsten, L; Cantiello, M; Dessart, L; Farmer, R; Hu, H; Langer, N; Townsend, RHD; Townsley, DM; Timmes, FX. “Modules for Experiments in Stellar Astrophysics (MESA): Binaries, Pulsations, and Explosions,” *ApJS*, v. 220, 2015, p. 15. http://adsabs.harvard.edu/abs/2015ApJS..220...15P

Paxton, B; Schwab, J; Bauer, EB; Bildsten, L; Blinnikov, S; Duffell, P; Farmer, R; Goldberg, JA; Marchant, P; Sorokina, E; Thoul, A; Townsend, RHD; Timmes, FX. “Modules for Experiments in Stellar Astrophysics (MESA): Convective Boundaries, Element Diffusion, and Massive Star Explosions,” *ApJS*, v. 234(2), 2018, p. 34. https://ui.adsabs.harvard.edu/abs/2018ApJS..234...34P

Paxton, B; Smolec, R; Schwab, J; Gautschy, A; Bildsten, L; Cantiello, M; Dotter, A; Farmer, R; Goldberg, JA; Jermyn, AS; Kanbur, SM; Marchant, P; Thoul, A; Townsend, RHD; Wolf, WM; Zhang, M; Timmes, FX. “Modules for Experiments in Stellar Astrophysics (MESA): Pulsating Variable Stars, Rotation, Convective Boundaries, and Energy Conservation,” *ApJS*, v. 243(1), 2019, p. 10. https://ui.adsabs.harvard.edu/abs/2019ApJS..243...10P

Prust, LJ; Chang, P. “Common envelope evolution on a moving mesh,” *MNRAS*, v. 486(4), 2019, p. 5809–5818. https://ui.adsabs.harvard.edu/abs/2019MNRAS.486.5809P

Ricker, PM; Taam, RE. “An AMR Study of the Common-envelope Phase of Binary Evolution,” *ApJ*, v. 746, 2012, p. 74. http://adsabs.harvard.edu/abs/2012ApJ...746...74R

Sabach, E; Hillel, S; Schreier, R; Soker, N. “Energy transport by convection in the common envelope evolution,” *MNRAS*, v. 472, 2017, p. 4361–4367. https://ui.adsabs.harvard.edu/abs/2017MNRAS.472.4361S

Soker, N. “What Planetary Nebulae Can Tell Us about Planetary Systems,” *ApJ*, v. 460, 1996, p. L53. https://ui.adsabs.harvard.edu/#abs/1996ApJ...460L..53S

Soker, N; Grichener, A; Sabach, E. “Radiating the hydrogen recombination energy during common envelope evolution,” preprint (arXiv:1805.08543), 2018, p. arXiv:1805.08543. https://ui.adsabs.harvard.edu/abs/2018arXiv180508543S

Springel, V. “E pur si muove: Galilean-invariant cosmological hydrodynamical simulations on a moving mesh,” *MNRAS*, v. 401, 2010, p. 791–851. http://adsabs.harvard.edu/abs/2010MNRAS.401..791S

Toro, E. *Riemann Solvers and Numerical Methods for Fluid Dynamics: A Practical Introduction*, Springer Berlin Heidelberg, ISBN 9783540498346, 2009

Turk, MJ; Smith, BD; Oishi, JS; Skory, S; Skillman, SW; Abel, T; Norman, ML. “yt: A Multi-code Analysis Toolkit for Astrophysical Simulation Data,” *The Astrophysical Journal Supplement Series*, v. 192, 2011, p. 9. http://adsabs.harvard.edu/abs/2011ApJS..192....9T

Webbink, RF. “Double white dwarfs as progenitors of R Coronae Borealis stars and Type I supernovae,” *ApJ*, v. 277, 1984, p. 355–360. http://adsabs.harvard.edu/abs/1984ApJ...277..355W

Zhu, C; Pakmor, R; van Kerkwijk, MH; Chang, P. “Magnetized Moving Mesh Merger of a Carbon-Oxygen White Dwarf Binary,” *ApJ*, v. 806, 2015, p. L1. http://adsabs.harvard.edu/abs/2015ApJ...806L...1Z